Stable water isotopes in pore water of Jurassic argillaceous rocks as tracers for solute transport over large spatial and temporal scales

T. Gimmi,[1,2] H. N. Waber,[1] A. Gautschi,[3] and A. Rübel[4,5]

Received 1 December 2005; revised 24 July 2006; accepted 13 November 2006; published 10 April 2007.

[1] In order to characterize the large-scale transport properties of the Opalinus Clay formation, the pore water isotope composition ($\delta^{18}O$ and $\delta^{2}H$) was determined on samples from the deep borehole Benken (northeastern Switzerland) across Jurassic argillaceous rocks. The sequence of claystones and marls, delimited by two aquifers, is located at depth from about 400 to 700 m and exhibits very low hydraulic conductivities (below 10^{-13} m s^{-1}). The isotope data of the pore water were obtained from core samples by diffusive vapor equilibration, vacuum distillation, and squeezing. Compared with the other methods, vacuum distillation led to too low values. To evaluate the large-scale transport properties of the formation, we performed a series of advective-dispersive model calculations and compared them with the experimental data. In accordance with the hydrogeological history, we varied initial and boundary conditions as well as model parameters. The main results can be summarized as follows: (1) Molecular diffusion to the underlying aquifer can explain the general features of the isotope profiles, (2) no signatures of advective flow could be detected, (3) the evolution time is of the order of 0.5–1 Ma (relying on laboratory diffusion coefficients) with a possible range of about 0.2–2 Ma, which is geologically plausible, and (4) parameters measured on small scales (centimeters or meters and months) are also plausible at the formation scale (tens of meters and millions of years) for the sediments investigated.

Citation: Gimmi, T., H. N. Waber, A. Gautschi, and A. Rübel (2007), Stable water isotopes in pore water of Jurassic argillaceous rocks as tracers for solute transport over large spatial and temporal scales, *Water Resour. Res.*, *43*, W04410, doi:10.1029/2005WR004774.

1. Introduction

[2] Claystones and marls typically have very low permeability. Consequently, they are widely considered as potential host rocks for the disposal of radioactive or other hazardous wastes. The barrier function of host rocks helps to retain wastes within the original disposal site and to minimize the risk of contamination of the biosphere.

[3] Transport properties of potential host rock formations are usually assessed by determining diffusion coefficients and permeabilities on small samples at laboratory scale, or by hydraulic tests in boreholes. Field experiments at larger scales in underground research laboratories complement the measurements and allow verifying of transport properties obtained at smaller scales. Performing experiments at scales of tens to hundreds of meters and thousands to millions of years, which are relevant in the case of disposal of radioactive waste is, however, impossible.

[4] In this situation, the analysis of natural isotope tracers offers unique possibilities. Their concentration patterns in pore fluids have developed over geologic time spans. Consideration of these patterns allows evaluating model concepts and material properties at relevant (i.e., formation) scales [e.g., *Desaulniers et al.*, 1981; *Remenda et al.*, 1996; *Hendry and Wassenaar*, 1999; *Rübel et al.*, 2002; *Pearson et al.*, 2003; *Patriarche et al.*, 2004a]. A perturbation of the chemical or hydraulic situation in an aquifer delimiting an aquitard can propagate through the latter. The characteristic time for the propagation and dissipation of the disturbance (and thus the time span over which a signature of the environmental tracers can be observed in the aquitard) depends on the extent and duration of the disturbance, and the physical and chemical properties of the rock. The latter factor is what we are interested in.

[5] The approach of using natural tracers has, unavoidably, some drawbacks. The "setups" of the "Experiments Performed by Nature" are not exactly known. Thus not only transport processes and parameters are unknown, but also boundary and initial conditions that are required for the interpretation of the data. In order to estimate which perturbations occurred in the past, one has to combine information about the regional paleohydrological and

[1]Rock-Water Interaction, Institute of Geological Sciences, University of Bern, Bern, Switzerland.
[2]Paul Scherrer Institut, Villigen, Switzerland.
[3]National Cooperative for the Disposal of Radioactive Waste, Wettingen, Switzerland.
[4]Institute for Environmental Physics, University of Heidelberg, Heidelberg, Germany.
[5]Now at Gesellschaft für Anlagen- und Reaktorsicherheit, Braunschweig, Germany.

0043-1397/07/2005WR004774$09.00

hydrochemical evolution. Because concentrations in the aquitard react slowly to perturbations at the boundaries, they may represent superpositions of several earlier events.

[6] Stable isotopes of water in pore water of argillaceous media proved to be useful in a number of cases. Most of the earlier studies focused on surficial Quaternary aquitards with relatively high porosities, where water samples could be obtained from wells. *Desaulniers et al.* [1981] investigated about 35 m of surficial till and clay deposits. From profiles of $\delta^{18}O$, $\delta^{2}H$, and chloride, they concluded that transport over the time since deposition (about 11–14 ka) was dominated by diffusion. Similar conclusions for $\delta^{18}O$ and $\delta^{2}H$ profiles in somewhat larger surficial Quaternary tills were obtained by *Remenda et al.* [1996] and *Hendry and Wassenaar* [1999]. The latter found diffusion-dominated profiles (evolution time of about 20–30 ka) also at the interface toward the underlying Cretaceous clay. Stable isotope contents in pore water of surficial clays and tills were further used to infer the paleoclimate, that is, the air temperature at the time of deposition [*Remenda et al.*, 1994], or the timing of climatic or hydrologic events [*Hendry and Wassenaar*, 1999].

[7] Over the last years, older formations were investigated as well. *Rübel et al.* [2002] presented pore water profiles of various tracers across Jurassic formations at the Mont Terri rock laboratory in the Jura mountains (northwestern Switzerland), where the formations can be accessed through a highway tunnel. As a result of the Jura folding and thrusting, the formations are tilted and exposed at the surface. On the basis of some limited modeling, *Rübel et al.* [2002] concluded that the He profile represents a steady state between diffusive loss and production, and that the stable water isotope profiles may have evolved by diffusion over a time span of about 10 Ma. However, the applied boundary conditions are very uncertain for the long time span. *Patriarche et al.* [2004a, 2004b] presented pore water concentrations of chloride and $\delta^{2}H$ in a sequence of Jurassic partly fractured aquifers and aquitards in southern France, accessible through an old railway tunnel. They attempted to model the Cl data over a time of 53 Ma, and applied the model also to the ^{2}H data. Diffusion seemed to play a major role, but the uncertainties with respect to the boundary conditions for this long time span and with respect to the local heterogeneities precluded a more detailed statement. In both studies it was assumed for the modeling that the profiles evolved from an initial seawater composition, neglecting possible earlier modifications of the pore water.

[8] Sampling water from wells is not possible in formations with very low permeabilities or at larger depths, and pore water data have to be obtained by indirect methods from core samples [*Kelln et al.*, 2001; *Sacchi et al.*, 2001; *Pearson et al.*, 2003; *Savoye et al.*, 2006]. While *Remenda et al.* [1994] partly applied squeezing, *Hendry and Wassenaar* [1999] (for part of the data) and *Patriarche et al.* [2004b] (for Cl^{-}) used radial diffusion cells with equilibration via a water phase. The $\delta^{2}H$ data used by *Patriarche et al.* [2004a] were obtained by vacuum distillation at 50°C. *Rübel et al.* [2002] developed a new water vapor equilibration technique, whereas *Hendry et al.* [2004] directly equilibrated the pore water in core samples with CO_2 or H_2 gas to determine detailed pore water isotope profiles. That technique was recommended by *Kelln et al.* [2001] in a comparison with squeezing, centrifugation, and azeotropic distillation, whereas diffusive equilibration via water or vapor phase proved to be well suited in other comparisons [*Hendry and Wassenaar*, 1999; *Pearson et al.*, 2003; *Savoye et al.*, 2006]. The method of *Rübel et al.* [2002], where the equilibration occurs via water vapor, has in our opinion some advantages, because the pore water chemistry is less disturbed as compared to direct equilibration with a solution of possibly different chemical composition, or to equilibration under possibly increased CO_2 or H_2 partial pressure.

[9] The aims of this study were to (1) apply the new method of *Rübel et al.* [2002] to obtain pore water isotope contents of tectonically undisturbed Jurassic rocks, (2) use these data to assess the relevant transport mechanisms (advection versus diffusion) in these rocks and (3) to estimate the formation-scale transport parameters, notably the diffusion coefficient, and (4) compare the formation-scale parameters with those obtained at smaller scales. For this purpose, we determined $\delta^{18}O$ and $\delta^{2}H$ values of pore water across more than 300 m of tectonically undisturbed Jurassic and uppermost Triassic formations. The formations with hydraulic conductivities below about 10^{-13} m s^{-1} are located at Benken in northeastern Switzerland at about 400 to 700 m below ground and include the Opalinus Clay as a potential host rock. They were accessed from the surface by a deep borehole [*Nationale Genossenschaft für die Lagerung radioaktiver Abfälle (Nagra)*, 2001, 2002]. The pore water data were obtained on core samples with the vapor equilibration method or, for comparison, with conventional vacuum distillation or squeezing.

[10] At the study site, the formations are sandwiched between two aquifers in the Malm and Keuper lithologies, respectively. Mass exchange processes with the aquifers have led to characteristic isotope signatures across the low-permeability zone that hint at diffusion-dominated transport. Because of the long time since deposition (~180 Ma) and because the formations are not exposed to the surface, it is not obvious which events created the signatures and what type of boundary and initial conditions should be applied. In particular, it is not clear whether constant boundary conditions as used by *Desaulniers et al.* [1981], *Remenda et al.* [1996], *Hendry and Wassenaar* [1999], and *Rübel et al.* [2002] in their studies are appropriate, and whether seawater can be used as initial condition for the modeling, as did *Rübel et al.* [2002] and *Patriarche et al.* [2004a]. Thus we tried to interpret the signatures by testing various partly time-dependent boundary and initial conditions for advective-diffusive transport models, which were inferred from the paleohydrology of the site.

2. Geology and Hydrogeology of Test Area

2.1. Geology

[11] The deep borehole was drilled at Benken (coordinates, reference system CH1903: 690′988.80/277′842.90, 404.30 m above sea level) in northeastern Switzerland. The study area is located in a tectonically quiet region between the northern boundary of the Swiss Molasse Basin and the Tabular Jura (Figure 1). A 3-D seismic survey [*Birkhäuser et al.*, 2001] revealed that the sedimentary rocks in the area are nearly horizontally bedded, and no faults were identified

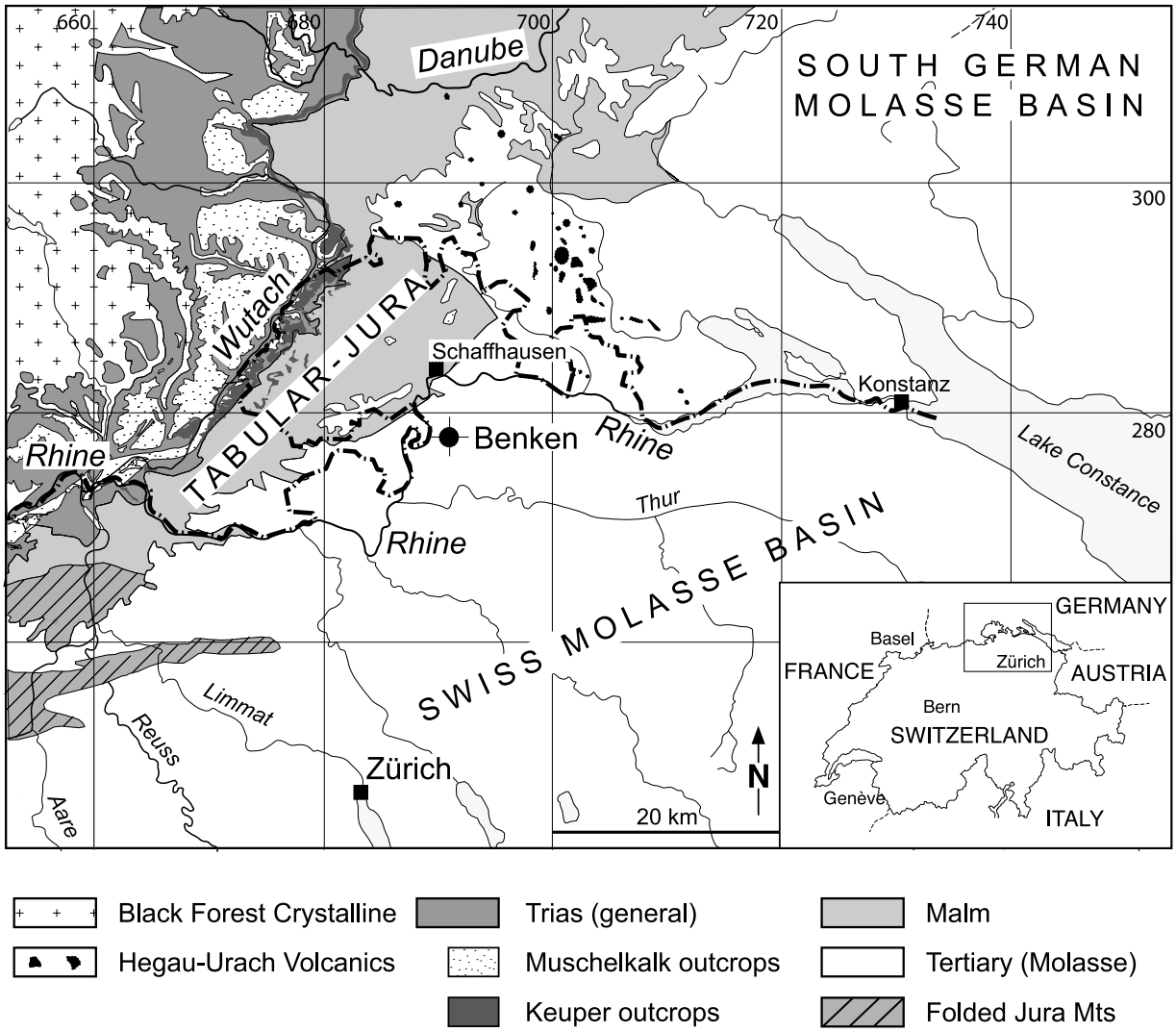

Figure 1. Simplified tectonic map of northeastern Switzerland and southwestern Germany showing the location of the Benken borehole. The numbers next to the grid lines indicate the coordinates (in km, reference system CH1903; Benken corresponds to 8.64957 longitude and 47.64492 latitude). The inset on the right shows the location of the study area within Switzerland and the neighboring countries.

(with a detection limit for vertical displacements of 10 m or 4 to 10 m for seismic attributes). On the basis of these results, the sequence of stratigraphic layers encountered in the Benken borehole is representative for the whole area.

[12] The lithostratigraphy encountered in the Benken borehole is summarized in Figure 2. Below the Tertiary, Malm, Dogger and Lias sediments of Jurassic age are encountered, indicating that the whole Cretaceous sequence was eroded. The Upper Malm comprises a 252-m-thick sequence of limestone with thin marl intercalations. The period of erosion during early Tertiary times resulted in a karstification of these limestone units. The underlying Dogger sediments consist of about 200 m of marine claystones and marls with intercalated thin layers of limestones, calcareous sandstones and iron ooliths. These sediments also contain the Opalinus Clay Formation which is (including the Murchisonae Beds in Opalinus Clay facies) a 113-m thick sequence of dark grey, silty and calcareous claystones. This unit is being investigated as a potential host rock for disposal of radioactive waste. Below, the Lias comprises about 40 m of marine marls, silt stones and claystones, and thin limestone beds. The upper third of the 119-m thick Triassic Keuper consists of sandy lithologies and dolomite breccias of the Stubensandstein and Schilfsandstein Formations, while the lower two thirds are made up of partly argillaceous anhydrite and gypsum layers and dolomites of the Gipskeuper.

[13] The Mesozoic sediment pile in northeastern Switzerland underwent a diagenetic overprint during two burial phases [*Mazurek et al.*, 2006]. A first, long-term burial occurred during Cretaceous times to a depth of about 1100 m, before about 600 m of sediment (Cretaceous and upper Malm) were eroded again during early Tertiary times (65–33.7 Ma B.P.). In the late Tertiary, the sediment pile was buried a second time to a depth of about 1700 m. This burial was shorter and reached its maximum about 10 Ma before present. Maximum temperatures of the two overprints were low, but greater during Cretaceous times (81 to 93°C) due to the longer burial. These events led to maturation of the organic material present in the rocks, carbonate cementation in the silty layers, limited recrystallization of

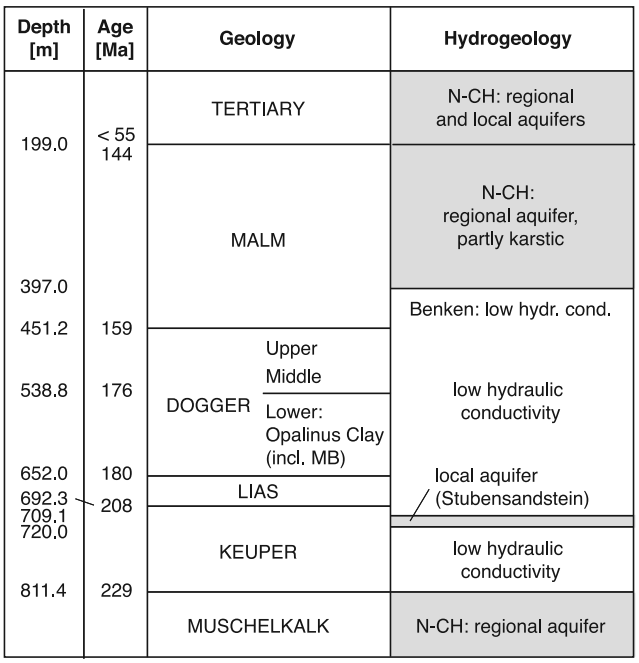

Figure 2. Simplified geologic and hydrostratigraphic division across the Benken borehole. N-CH, northern Switzerland; MB, Murchisonae Beds.

clay minerals, and the formation and mineralization of veins. In the Benken drill core only few open structures were observed in limestones, dolomites and sandstones, while veins are generally closed in the claystones, marls, and the gypsum-anhydrite layers [*Nagra*, 2002, p. 256ff].

2.2. Present and Past Hydrogeology

[14] Certain lithologies of the Malm constitute regional aquifers with commonly large groundwater production rates in northern Switzerland and adjacent southern Germany [*Pearson et al.*, 1991; *Bertleff and Watzel*, 2002]. The alluvial Keuper lithologies, in contrast, form aquifers of only local extent due to their high lateral variability [*Pearson et al.*, 1991]. The argillaceous rocks of the Dogger and Lias act as confining layers between these aquifers (Figure 2).

2.2.1. Malm

[15] Karstification of the Malm limestones during early Tertiary times resulted in a complex flow regime characteristic for such environments. The present hydraulic conductivity of Malm limestones is highly variable with values between 10^{-14} and 10^{-4}m s^{-1} and 10^{-14} to 10^{-9}m s^{-1} measured in the Benken borehole [*Nagra*, 2002, pp. 111f, 182f]. Major infiltration areas for the Malm aquifer (see Figure 1) are in the north from the river Rhine to the river Danube (Donau) and in the Folded Jura mountains to the west. Indirect infiltration through the Molasse sediments takes place in the south [*Balderer*, 1990]. Discharge from the Malm aquifer occurs into the river Danube to the east and into the river Rhine to the north and west of the study area with the water divide being east of the Lake Constance [*Bertleff and Watzel*, 2002; *Nagra*, 2002, p. 111f]. It should be noted that the present flow direction of the Rhine river was established around the Pliocene-Pleistocene boundary (2.7 Ma B.P.) when it changed from northeast toward the river Danube to west toward the Aare River [*Villinger*, 2003]. First discharge from the Malm limestones into the Rhine river is thought to have occurred in the early Pleistocene (about 1.8–2 Ma B.P.) when the river eroded into these limestones.

[16] The evolution of Malm groundwater has to be interpreted within the complex paleohydrologic history from Jurassic to present times. The original formation water was seawater. Erosion of the overlying Cretaceous marine sediments and subsequent karstification of the Malm limestones resulted in the first dilution of the marine-type formation water with fresh water during the early Tertiary times (about 65–33.7 Ma B.P.). The succeeding deposition (about 30–10 Ma B.P.) of up to 6000 m of Tertiary Molasse sediments in four alternating freshwater and marine to brackish water cycles gave rise to a complex mixture of freshwater and marine water components.

2.2.2. Keuper

[17] In the Keuper aquifer the hydraulic continuity within an individual stratigraphic unit is limited due to pronounced lateral differences in lithology. This is confirmed by the lateral variability of the hydraulic conductivity of an individual unit (10^{-10} to 10^{-7}m s^{-1}) and by the fact, that the water-conducting zone is different in different boreholes in the region [*Pearson et al.*, 1991; *Nagra*, 2002, p. 114f]. On a regional scale, groundwater flow in the Keuper occurs due to a hydraulic connection of these individual units, which are all bound by the overlying Liassic claystones and marls and underlying evaporite layers of the Keuper. A conceptual flow model suggests the foothills of the Black Forest east of the river Wutach as the major infiltration area. Discharge of groundwater from the Keuper water-conducting zones occurs westward in the river Rhine [*Nagra*, 2002, p. 114f]. In the study area, the water-conducting zone of the Keuper is the Stubensandstein Formation, which consists of sandy layers at the bottom and dolomite breccias at the top with a hydraulic conductivity of about 10^{-7}m s^{-1} [*Nagra*, 2002, p. 114f]. The porous dolomite breccias are the result of the dissolution of evaporitic layers during diagenesis. The discharge zones for the Keuper aquifer that are still active today were probably created by deep erosion in the Klettgau area (to the west of the study site) some 1.8 Ma ago following the diversion of the Alpenrhein toward the Aare river, which occurred about 2.7 Ma B.P. [*Villinger*, 2003]. The change in flow direction also coincides about with the exhumation of the Keuper lithologies and direct infiltration into these.

2.2.3. Dogger and Lias

[18] In the Dogger and Lias formations between Malm and Keuper very low hydraulic conductivities (in general below 10^{-13}m s^{-1} (borehole injection tests of *Nagra* [2002, p. 112f])) were measured. They resulted from the compaction of the marine, clayey sediments during the two burial events, which reduced drastically the typical pore sizes as well as the porosity. Only very low flow velocities (about 3 m Ma^{-1}, see section 5.6.) are estimated for these formations based on present-day hydraulic gradients.

3. Experimental Data

3.1. Sampling and Pore Water Analysis

[19] Groundwater from the Malm and the Keuper could be collected from packed-off intervals in the borehole. No such sampling was possible for the layers in between. From

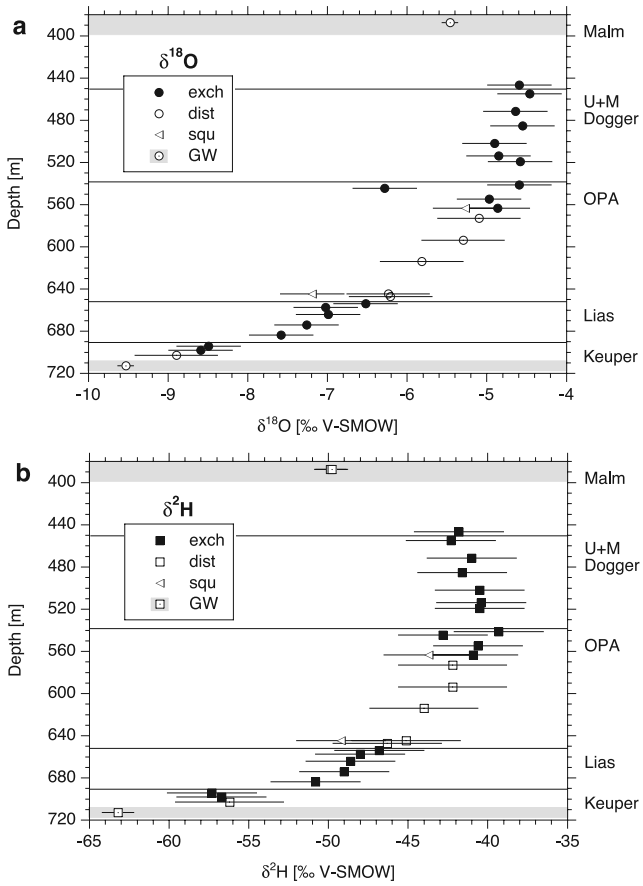

Figure 3. Profiles of (a) $\delta^{18}O$ and (b) $\delta^{2}H$ in the pore water across the Benken borehole (exch, diffusive exchange; dist, corrected distillation; squ, squeezing; GW, groundwater).

depths between about 450 and 700 m, core samples with lengths of about 30 cm and diameters of about 10 cm were brought to the surface and immediately sealed under N_2 atmosphere in vapor-tight polyethylene-coated aluminum bags. The samples were kept under cool conditions and brought to the laboratory within a few days and then immediately processed.

[20] The isotopic composition of pore water in cores was determined using different methods: the commonly used vacuum distillation, the diffusive vapor exchange [*Rübel et al.*, 2002], and (for two samples) high-pressure squeezing. For all methods the rim of the core (ca. 1 to 2 cm), which might have been contaminated by drilling fluid, was removed. For the vacuum distillation method the central part of the core was placed into vacuum containers. The pore water was removed from the rock samples over a period of 48 h under vacuum at 105°C and directly analyzed in the mass spectrometer. For the diffusive exchange method, rock pieces of about 1 cm^3 were placed into a vapor-tight container together with a small amount of test water with known initial isotope composition. Diffusive exchange between the two fluid reservoirs (pore water and test water) via the vapor phase led finally to equal isotopic compositions in both reservoirs. Water condensation on container walls or swelling of the sample was prevented, as checked by weighing, by adding some NaCl to the test solution. Fractionation effects between pore water and test water are negligible for the given water contents and differences in salinity [*Rübel et al.*, 2002]. Making two such experiments with different initial concentrations of the test water allows calculating both the original isotopic composition of the pore water and the water content of the rock sample from the final concentrations of the test water. Details of both methods are given by *Rübel et al.* [2002]. Furthermore, two water samples were obtained by squeezing at 512 MPa a rock sample tailored to 50 mm diameter and 70 mm height. The amount of water obtained in this way corresponded to about 12 and 19%, respectively, of the pore water [*Nagra*, 2002].

[21] The ^{18}O and ^{2}H values of all water samples were determined using standard mass spectrometric procedures. All data are presented in the usual δ notation relative to the Vienna Standard Mean Ocean Water (VSMOW).

[22] A comparison between the diffusive exchange and the distillation method clearly revealed that the latter consistently underestimated the ^{18}O and ^{2}H values in the pore fluid. The distillation data were, on average, lower by 2.9 ± 0.33‰ in $\delta^{18}O$ and 10.7 ± 1.9‰ in $\delta^{2}H$. This phenomenon is commonly observed for clayey samples [*Kelln et al.*, 2001; *Rübel et al.*, 2002; *Pearson et al.*, 2003; *Savoye et al.*, 2006], and is attributed to the incomplete removal and a Rayleigh-type fractionation of the pore water during distillation, which leads to a depletion of heavy isotopes in the extracted water. This interpretation is also supported by the good agreement of the squeezing and the diffusive exchange (but not the uncorrected distillation) data (see Figure 3). In the following we will therefore focus on the data from diffusive exchange. Unfortunately, no diffusive exchange data between about 570 and 650 m were obtained because of a handling error (inadequate test water used). In this range, distillation data, shifted by the mean deviation between the two data sets mentioned above are shown.

[23] The accuracy of the mass spectrometer measurements and of the ground water samples is ±0.1‰ for $\delta^{18}O$ and ±1.0‰ for $\delta^{2}H$. Errors of the pore water values obtained with the diffusive exchange method were estimated to be ±0.4‰ for $\delta^{18}O$ and ±2.8‰ for $\delta^{2}H$ based on first-order error propagation. Similar errors were attributed to the squeezing data. Somewhat larger errors of ±0.5‰ for $\delta^{18}O$ and ±3.4‰ for $\delta^{2}H$ were calculated for the shifted distillation data, based on first-order error propagation and assuming identical statistical errors for the distillation as for the diffusive exchange method.

3.2. Profiles of $\delta^{18}O$ and $\delta^{2}H$

[24] Figure 3 shows profiles of $\delta^{18}O$ and $\delta^{2}H$ in the pore water across the low-permeability zones at Benken, together with the values of the groundwater in the bounding aquifers. Figure 4 displays the relations between the $\delta^{18}O$ and $\delta^{2}H$ data (vapor equilibration, squeezing, and corrected distillation data). The following observations can be made: (1) The profiles of $\delta^{18}O$ and $\delta^{2}H$ have similar shapes. The values are largest near the center and upper half of the Dogger units and decrease toward the Keuper aquifer. (2) The groundwater data match well with the values of the adjacent low-permeability zones. (3) The shifted distillation data fit well into the profiles of the diffusive exchange data. (4) The two squeezing data match, within the errors, with the other data. (5) The isotopic composition of pore water in the Dogger

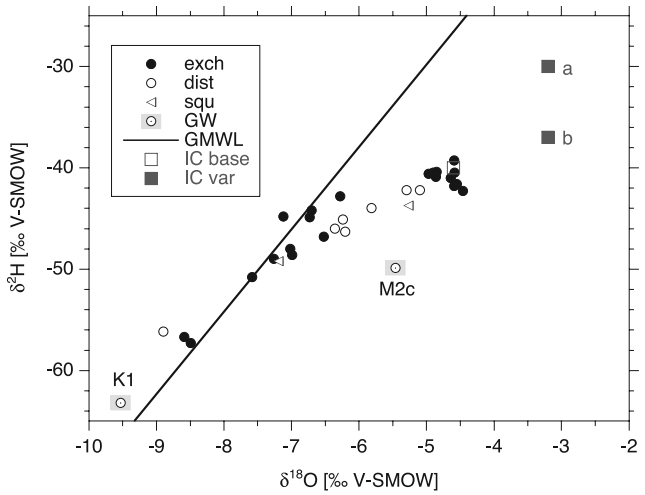

Figure 4. Relationship between the $\delta^{18}O$ and $\delta^{2}H$ contents of pore water and groundwater from the Benken borehole (exch, diffusive exchange; dist, corrected distillation; squ, squeezing; GW, groundwater; GMWL, global meteoric water line; K1, Keuper; M2c, Malm). Also shown are initial conditions used later in the modeling (IC base and IC var a and b).

units is generally heavier than that of modern meteoric waters, and lighter than initial pore water, which was seawater. (6) On a plot of $\delta^{2}H$ versus $\delta^{18}O$ (Figure 4), the data for the greater depths lie on the Global Meteoric Water Line, whereas those above about 650 m (i.e., the Dogger sediments) lie to the right of it.

[25] The $\delta^{18}O$ value at about 545 m deviates considerably from values for neighboring samples while the $\delta^{2}H$ value differs only slightly from neighboring values. The reason for the relatively low values at about 545 m is unclear. Neither hydraulic conductivities in this zone, nor structure or mineral composition of that sample, have revealed any differences to the surrounding zones. Thus it seems unlikely that the relatively low values originate from locally altered (hydro)geologic properties, and the data are treated as outliers, originating possibly from an analytical or sampling artefact.

3.3. Porosities

[26] Water content porosities between 0.07 and 0.17 m^3 m^{-3} (mean of 0.13 ± 0.028 m^3 m^{-3}) were obtained for the samples with the diffusive exchange method. The values (Figure 5, solid symbols) match well with the porosity estimates of the geophysical borehole logs [*Nagra*, 2001] and are larger by about 15% than those from distillation (Figure 5, open symbols). The latter is in accordance with the findings of *Rübel et al.* [2002] and with the interpretation that distillation was incomplete.

4. Modeling Approaches

4.1. Geologic Scenarios

[27] The originally deposited marine water had values probably in the range between −2 and 0‰ [e.g., *Gregory*, 1991]. The measured isotopic composition of the Dogger pore waters represents a remnant from marine formation water diluted by younger meteoric water. In view of the very long timescale (more than 144 Ma since deposition)

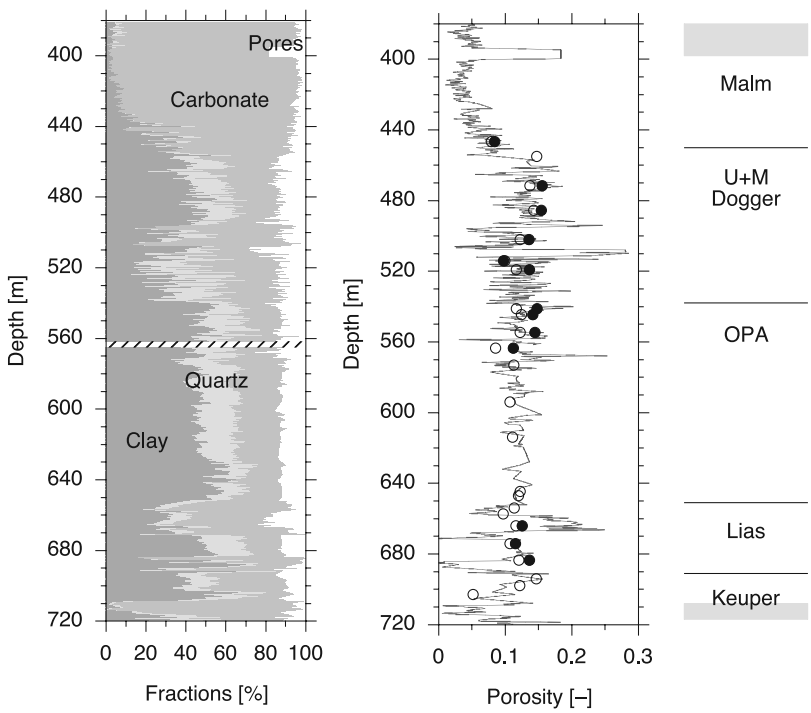

Figure 5. Mineralogy and porosity of the Benken borehole calculated from geophysical borehole logs and porosities for the samples from which the stable isotope values were obtained (solid symbols, from diffusive exchange; open symbols, from vacuum distillation; hatched line in Figure 5 (left), no borehole log data).

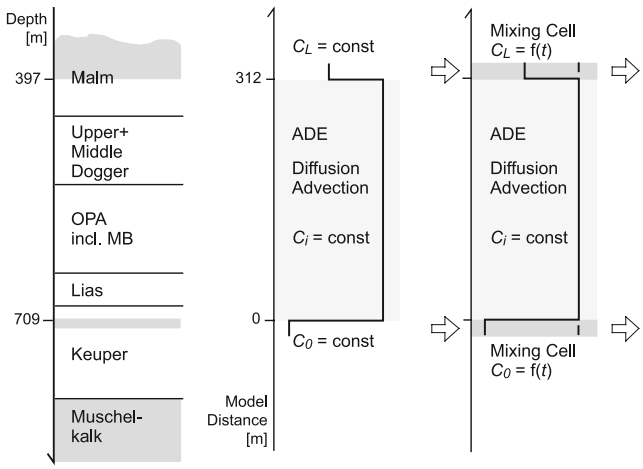

Figure 6. Schematic representation of the model setup chosen and the corresponding boundary and initial conditions.

and the uncertainties in geologic history, we did not attempt to model the detailed development of the isotopic concentrations in pore water since deposition. Instead, we concentrate on the most dominant feature of the data, which is the decrease of δ values from the Dogger toward the Keuper.

[28] Today, the low-permeability formations are sandwiched between two aquifers, the Malm and the Stubensandstein Formation in the Keuper. These aquifers define the upper and the lower boundaries of the modeled domain (Figure 6). In view of the large lateral extent and the undisturbed structure of the geologic strata in the Benken area, a one-dimensional approach was chosen.

[29] The basic hypothesis is that the shape of the profile originates from a relatively late change in the Keuper boundary condition. Diffusive and possibly also advective transport has then propagated the perturbation of isotopic concentrations at the lower boundary into the Dogger units. This scenario is consistent with the (hydro)geologic history presented in Section 2. In the following paragraphs, we derive the corresponding boundary and initial conditions for our modeling.

4.1.1. Initial Conditions

[30] Jurassic (206–144 Ma B.P.) and Cretaceous (144–65 Ma B.P.) sediments were deposited mainly under marine conditions. After erosion of Cretaceous as well as upper Malm layers, the lower Malm was karstified and exposed to fresh water for at least 30 million years (about 65–33.7 Ma B.P.). About 30–10 Ma ago, the Jurassic sediments were covered again by the Molasse sediments, which comprise a sequence of alternating fresh and marine water sediments.

[31] The changing upper boundary conditions, and the long time spans involved, most likely resulted in rather smooth, low-gradient concentration profiles across the Jurassic sediments. This means that the isotopic concentrations across most of the Dogger units were approximately constant, but at an unknown value, before the relatively late event generated the shapes observed today.

4.1.2. Keuper Boundary Condition

[32] The water-conducting zone of the Keuper in Benken, the Stubensandstein Formation, is about 11 m thick and consists of porous dolomite breccia at the top. They are the result of the dissolution of evaporitic layers during diagenesis. Thus the permeability of this layer was much lower than it is at present for a very long period of time.

[33] Direct infiltration into the Keuper lithologies occurs at present in the Wutach region to the north of Benken (section 2.2.2 and Figure 1). Discharge zones were created some 1.8–2.0 Ma ago following the diversion of the Alpenrhein toward the Aare river [*Villinger*, 2003].

[34] It thus appears that the Keuper units contained old formation water and had similar hydraulic properties as the overlying Dogger units for most of the time since deposition. Significant flushing with meteoric water may have started less than about 2 Ma ago with the creation of new discharge areas. The flushing with meteoric water led then to the drop in the concentration of stable water isotopes.

[35] This scenario is also supported by the Keuper water sampled [*Nagra*, 2002, p. 195ff]. Chemical and isotopic composition of this water consistently indicate an evolution in the formation from which it was sampled (i.e., Stubensandstein) and an infiltration under climatic conditions like those of the present. The absence of measurable tritium excludes the presence of a young groundwater component, and the undetectable ^{14}C, the high He content, and the high $^{40}Ar/^{36}Ar$ ratio of this water indicate that recharge occurred well before the present climatic period, most probably during early Pleistocene times [*Gimmi and Waber*, 2004]. Although no absolute age can be derived for the Keuper water, the water chemistry limits its residence time in the subsurface to an interval between 2.6 Ma (interglacial climate) and substantially more than 25,000 years (high He and radiogenic Ar concentrations, absence of ^{14}C).

[36] From the geology and the water chemistry it can be concluded that the evolution time of the profiles in the low-permeability zones, that is the time since the concentration dropped in the Keuper aquifer in Benken, must be lower than about 1.8 Ma when direct infiltration and regional discharge to the present Rhine were established. The stable isotope signature of the Keuper aquifer in Benken may have varied somewhat with time since then, with lower values resulting from infiltration during the glacial periods.

4.1.3. Malm Boundary Condition

[37] The fact that the whole sequence of Cretaceous sediments was eroded in the area and that the Malm limestones are strongly karstified suggest that the original marine formation water was flushed before Tertiary times. During the Tertiary, the area was subjected to alternating fresh water and brackish to seawater environments under subtropical to tropical conditions [*Trümpy*, 1980] and the Malm could possibly have been saturated alternately with seawater and fresh water. An explanation of the Malm groundwater that is consistent with the measured data is that it is a mixture of a Tertiary seawater component with meteoric water [*Gimmi and Waber*, 2004]. The age of this meteoric component is difficult to define. Radiogenic and stable isotopes and noble gases suggest, however, that infiltration of this meteoric component must have occurred at least during an interglacial period in the early Pleistocene if not during late Tertiary times. At present, the entire sequence of Malm limestones at Benken is characterized by a low hydraulic conductivity and almost stagnant groundwater flow conditions can be assumed over this entire time range. Because of the complex paleohydrogeo-

logic evolution of the Malm groundwater it is difficult to define unique boundary conditions. Thus we will test various sets.

4.1.4. Spatial and Temporal Variability of Parameters

[38] Structural and mineralogical investigations of rock samples across the Dogger units have revealed a relatively small spatial variability [*Nagra*, 2001]. Only in a few locations with a small vertical extent were there clear differences in porosity or mineralogy (with the exception of the lower Malm), as can be seen for instance from the mineralogy or porosity calculated based on several calibrated geophysical borehole logs [*Nagra*, 2001] or from the porosity values of the samples used to derive the stable water isotope values (Figure 5). In view of the relatively small variability it seems justified to assume spatially constant transport parameters throughout the entire domain. As a check, some calculations were also run for heterogeneous porosities and diffusion coefficients.

[39] Properties of the domain will certainly have changed with time since deposition. Strong compaction of the clayey sediments occurred during two subsequent burial events during the Cretaceous and Tertiary. This compaction can be considered as nearly irreversible, in that probably no dramatic changes of the rock fabric took place during the last 10 Ma or so, where the whole area was generally lifted up. There also is no evidence that the relatively late contact with fresh Keuper water altered the structure of the sediments significantly, because porosity, for instance, shows only a slight trend with depth. Thus we will also assume temporally constant parameters.

4.2. Transport Equations

[40] The δ values used for isotopes are scaled and shifted ratios of two isotope concentrations and thus depend on both of them:

$$\delta = \frac{R}{R_{std}} - 1 = \frac{{}^bC}{{}^aC}\left(\frac{{}^aC}{{}^bC}\right)_{std} - 1, \tag{1}$$

where $R = {}^bC/{}^aC$, ${}^aC$ and ${}^bC$ are the concentrations of the main or reference isotope a and of the less abundant isotope b, respectively, and *std* denotes values of the standard. In case of water isotopes, the total water concentration and thus also ${}^aC$ remains (for the temperatures and pressures considered) essentially constant in time and space. Then, the δ values just represent linearly scaled and shifted concentrations of the isotope b and can be treated in the differential transport equations as any ordinary chemical concentration C.

[41] Following the arguments presented in section 4.1., transport calculations were generally based on the one-dimensional advective-dispersive equation with constant coefficients

$$\frac{\partial C}{\partial t} = D_p \frac{\partial^2 C}{\partial z^2} - v\frac{\partial C}{\partial z}, \tag{2}$$

where C is the concentration or δ value of an isotope in the water phase, D_p is the (pore) dispersion coefficient, v the average linear pore velocity, t the time, and z the depth coordinate (positive upward with $z = 0$ at 709.1 m below ground, $z = L$ at 397.0 m below ground, and $L = 312.1$ m; see Figure 6). Note that the porosity or water content ε was assumed to be about constant throughout the formations and therefore could be eliminated. For very low advective velocities, as expected in such clay layers, dispersion is dominated by diffusion, and D_p is just the pore diffusion coefficient. Note that D_p does not include the porosity, in contrast to the so-called effective diffusion coefficient D_e [e.g., *Flury and Gimmi*, 2002].

4.2.1. Initial and Boundary Conditions

[42] Initially, uniform isotope concentrations throughout the modeled domain ($0 \le z \le L$) were assumed. As first estimates, we used initial values of $\delta^{18}O = -4.6‰$ and $\delta^2H = -40‰$ according to maximum values observed today in the upper Dogger units. Alternatively, larger initial concentrations of $\delta^{18}O = -3.2‰$ and $\delta^2H = -30$ or $-37‰$ were tested, representing pore waters less diluted by fresh water. The larger initial value for $\delta^{18}O$ was chosen more or less arbitrarily. The values for δ^2H were then selected either so that a similar fit as for $\delta^{18}O$ was obtained at similar times, or according to the trend of the relation between $\delta^{18}O$ and δ^2H in the upper part of the profile (see Figure 4).

[43] The concentration drop at the lower boundary at $t = 0$ was modeled in two different ways. The first was simply to assume that constant concentrations C_0 have prevailed at $z = 0$ since the flushing of the aquifer ($t > 0$), equal to the values measured today in the Keuper aquifer ($\delta^{18}O = -9.53‰$ and $\delta^2H = -63.2‰$). The second takes into account a gradual decrease from initial values in the Keuper aquifer, equal to the initial values in the pore water, to those observed today, as may have happened during the increase of the hydraulic conductivity and the onset of flow. The gradual decrease was achieved by representing the aquifer as a mixing cell of equivalent height ζ, which was flushed for $t > 0$ at a given rate ρ with water of a given concentration C_{in}. The concentration drop in this mixing cell, in which concentrations are always uniform, results from the interplay of advective and diffusive mass transfer across the boundary to the low-permeability zone, and advective input and output of flushing water. The equation for the lower boundary is in this case

$$\varepsilon_m V\frac{\partial C_m}{\partial t} = \varepsilon_m A v_{in} C_{in} - \varepsilon_m A v_{out} C_m - \varepsilon B\left(vC|_{z=0} - D_p\frac{\partial C}{\partial z}\bigg|_{z=0}\right), \tag{3}$$

where C_m is the concentration within the mixing cell (aquifer), V the volume, A the vertical, and B the horizontal cross sectional area of the mixing cell over which solute exchange happens, ε_m the porosity of the aquifer, C_{in} the concentration of the flushing water, v_{in} the flushing velocity, and v_{out} the velocity of the water leaving the mixing cell. Taking into account the mass balance for water and neglecting density changes, v_{out} is related to v and v_{in} as $v_{out} = v_{in} - v(\varepsilon B)/(\varepsilon_m A)$ (for z positive upward). Using this relation and introducing the flushing rate

$$\rho \equiv v_{in}A/V \tag{4}$$

and the equivalent height of the aquifer or mixing cell

$$\zeta \equiv \varepsilon_m V/(\varepsilon B), \tag{5}$$

the equation for the mixing cell can be simplified to

$$\frac{\partial C_m}{\partial t} = \rho(C_{in} - C_m) + \frac{D_p}{\zeta}\frac{\partial C}{\partial z}\bigg|_{z=0}. \quad (6)$$

[44] To obtain this last equation, we assumed continuity of concentrations across the lower boundary, i.e., $C_m = C(z = 0, t)$. This assumption together with the use of a dispersive and an advective term for mass transfer between aquifer and low-permeability layers in equation (3) corresponds to a resident injection, as defined by *Gimmi and Flühler* [1998]. This type of solute exchange is typical for a reservoir in close contact with an advective-dispersive transport domain and for low advective velocities. We assumed meteoric concentrations of the flushing water C_{in} of $\delta^{18}O = -9.53‰$ and $\delta^{2}H = -63.2‰$ or slightly lower values, accounting for a glacial input, and investigated various flushing rates ρ.

[45] For the Malm interface at $z = L$, the following boundary conditions were compared: Constant concentrations C_L according to measured values of the Malm aquifer ($-5.46‰$ and $-49.8‰$) that may have prevailed for several hundreds of thousands to a few millions of years, zero concentration gradients at $z = L$, or a mixing cell boundary condition analogous to that at the lower interface.

4.2.2. Solutions

[46] To be flexible with respect to boundary conditions, we obtained solutions generally in Laplace space and inverted them back numerically with the Talbot algorithm [*Jury and Roth*, 1990]. A numerical finite difference code was used in addition to check some specific scenarios. The Laplace space solution for constant concentrations $C(0,t) = C_0$ and $C(L,t) = C_L$ is

$$\widehat{C}(z;s) = \frac{(C_L - C_i)e^{a(z-L)}\sinh(abz)}{s\,\sinh(abL)} - \frac{(C_0 - C_i)e^{az}\sinh[ab(z-L)]}{s\,\sinh(abL)} + \frac{C_i}{s}, \quad (7)$$

where C_i is the initial concentration, $a \equiv v/(2D_p)$, $b \equiv (1+4\ s\ D_p/v^2)^{1/2}$, $\widehat{\ }$ denotes a Laplace transformed variable, and s is conjugate to time t.

[47] The solution for a constant concentration $C(0,t) = C_0$ and a zero gradient at $z = L$ is

$$\widehat{C}(z;s) = \frac{b\cosh[ab(z-L)] - \sinh[ab(z-L)]}{b\cosh(abL) + \sinh(abL)} \times \frac{(C_0 - Ci)}{s}\ e^{az} + \frac{C_i}{s}. \quad (8)$$

[48] For a mixing cell at $z = 0$ with $C(0, t) = C_m(t)$, and a constant concentration $C(L, t) = C_L$, a zero gradient, or another mixing cell with $C(L, t) = C_{mL}(t)$ at $z = L$, the general Laplace space solution is

$$\widehat{C}(z;s) = A_1 e^{az(1+b)} + A_2 e^{az(1-b)} + \frac{C_i}{s}. \quad (9)$$

For a constant concentration $C(L,t) = C_L$ at $z = L$ and the mixing cell at $z = 0$, the coefficients in the above equation are

$$A_1 = \frac{T_2(C_L - C_i)e^{-aL(1-b)} - T_3}{s(T_2 e^{2abL} - T_1)}, \quad A_2 = \frac{T_3 - T_1(C_L - C_i)e^{-aL(1+b)}}{s(T_2 - T_1 e^{-2abL})} \quad (10)$$

with

$$T_1 = \rho + s - \frac{v(1+b)}{2\zeta},\ T_2 = \rho + s - \frac{v(1-b)}{2\zeta},\ T_3 = \rho C_{in} + sC_{mi} - (\rho + s)C_i,$$

where ρ is the flushing rate defined in equation (4), ζ the equivalent height or thickness of the mixing cell defined in equation (5), and C_{mi} the initial concentration in the mixing cell.

[49] For a zero gradient at $z = L$ and the mixing cell at $z = 0$, the coefficients are

$$A_1 = \frac{T_3(1-b)}{s(T_1[1-b] - T_2[1+b]e^{2abL})}, \quad A_2 = \frac{T_3(1+b)}{s(T_2[1+b] - T_1[1-b]e^{-2abL})} \quad (11)$$

with T_1, T_2, and T_3 as above.

[50] Finally, for mixing cells at both ends, the following coefficients can be found:

$$A_1 = \frac{T_3 T_{2L} e^{aL(1-b)} - T_2 T_{3L}}{s(T_1 T_{2L} e^{aL(1-b)} - T_2 T_{1L} e^{aL(1+b)})}, \quad A_2 = \frac{T_1 T_{3L} - T_3 T_{1L} e^{aL(1+b)}}{s(T_1 T_{2L} e^{aL(1-b)} - T_2 T_{1L} e^{aL(1+b)})} \quad (12)$$

with T_1, T_2, and T_3 as above, and

$$T_{1L} = \rho_L + s + \frac{v(1+b)}{2\zeta_L},\ T_{2L} = \rho_L + s + \frac{v(1-b)}{2\zeta_L},\ T_{3L} = \rho_L C_{inL} + sC_{miL} - (\rho_L + s)C_i,$$

where ρ_L, ζ_L, C_{inL}, and C_{miL} are the flushing rate, the equivalent height or thickness, the inflowing concentration, and the initial concentration of the mixing cell at $z = L$, respectively. Switching boundary conditions between $z = 0$ and $z = L$ is possible, if required, by switching the direction of the z axis. For velocities $v \to 0$ or, correspondingly, Peclet numbers $Pe = v\,L/D_p \ll 1$, the above solutions tend to the solutions for pure diffusion.

4.3. Parameter Estimation

[51] The dispersion coefficient D_p and the advective flow velocity v in the low-permeability zone were initially treated as unknowns, although we have some information about small-scale diffusion coefficients of Opalinus Clay samples and present-day hydraulic properties in the Benken area. We do not know precisely, when the concentration drop in the Keuper aquifer occurred. Thus the evolution time t was also considered as an unknown. It is then convenient to replace

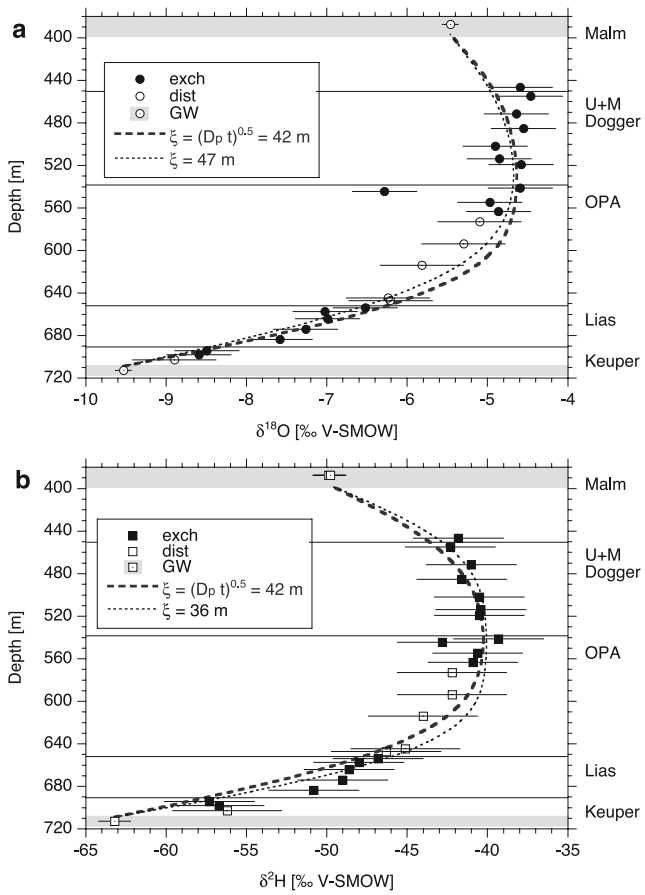

Figure 7. Best fit simulations for the (a) $\delta^{18}O$ and (b) $\delta^{2}H$ data for the base case (pure diffusion, constant concentrations at Keuper and Malm boundary, initial concentrations derived from maximum concentrations found in pore water). Thick lines, best fit for combined $\delta^{18}O$ and $\delta^{2}H$ data sets; thin lines, individual best fits for each data set.

the time t in the transport equation with a dimensionless diffusion time $T_D = D_p\ t/L^2$, where L is the size of the domain, or, since L is known, with a diffusion distance $\xi = (D_p\ t)^{1/2}$. Consequently, for $v = 0$ the transport equation has no free parameter, and the concentrations C are a function of the dimensionless variables T_D and z/L, or of the lengths ξ and z only. If v is different from zero, the transport equation depends on a single parameter, namely the Peclet number $Pe = v\ L/D_p$ in case of T_D, or the dispersivity D_p/v in case of ξ. If a mixing cell boundary condition is used, equation (6) has to be transformed as well such that instead of the flushing rate ρ a scaled parameter $\rho\ L^2/D_p$ or ρ/D_p, respectively, appears.

[52] In the following, we will express concentrations as a function of the diffusion distance ξ. We will try to estimate ξ and D_p/v from the ^{18}O and ^{2}H data sets. For that purpose, the weighted sum of squares of the deviations between measured and calculated data, the χ^2 function, is minimized (ignoring the values at 545 m). As a criterion to assess the relative quality of the fit of a simulation, we used the calculated χ^2 divided by the number of data points n

$$\Delta \equiv \frac{\chi^2}{n} = \frac{1}{n}\sum_{i=1}^{n}\frac{(y_i - y_{ci})^2}{\sigma_i^2} \qquad (13)$$

where y_i are measured and y_{ci} calculated values, and σ_i is the standard deviation of the measurements. The quantity Δ gives the average squared deviation between the measurements and the simulations, scaled by the variance.

[53] Since oxygen and hydrogen in water generally move together as a water molecule, it makes sense to combine the two data sets for parameter estimation. In this case, equal weight was attributed to each set. We also estimated parameters for each data set individually. Once a value of $\xi = (D_p\ t)^{1/2}$ was obtained, we could use laboratory-scale diffusion coefficients of Opalinus Clay to estimate the time that has passed since the concentration in the Keuper aquifer dropped, or, the other way round, obtain diffusion coefficients, provided evolution times were known a priori.

5. Modeling Results and Discussion

5.1. Base Case

[54] As a base case, we considered purely diffusive transport with constant concentrations for $t > 0$ according to present-day values at the Keuper and Malm boundaries. The initial values were derived from maximum values in the upper part of the domain. Figure 7 shows best fit curves for the combined ^{18}O and ^{2}H data sets (thick lines) for this base case. Minimum deviations between measurements and simulations were found for $\xi = 42$ m. Note that the data at about 545 m were ignored for the estimation of ξ.

[55] In general, the simulations for the base case with purely diffusive exchange match the data quite well. This indicates that the chosen setup with constant parameters, homogeneous initial conditions, and constant boundary concentrations is a possible scenario. Of course, some of the deviations between the data and the simulations may be linked to simplifications of the setup. For instance, the $\delta^{2}H$ values in the Lias, and to a lesser degree also the $\delta^{18}O$ values, have a gradient smaller than simulated around 660 m, and larger than simulated between about 680 and 710 m. This may point to larger than average porosity or D_p in the upper part of the Lias, and smaller than average in the lower part. Indeed, a somewhat larger porosity was estimated from the bulk densities obtained in the borehole log in the upper Lias (but not confirmed by the porosity values of the corresponding samples), as can be seen in Figure 5. The porosities obtained in the borehole log may suffer from local borehole collapse. Nevertheless, we ran simulations with a numerical code, taking into account the spatial heterogeneity of the porosity according to Figure 5, while assuming constant D_p. The simulations (not shown) revealed that this variability has only a small influence on the simulations and the estimated ξ values, but locally may improve the correspondence between measurements and simulations.

[56] In laboratory experiments on small Opalinus Clay samples from Benken, *Van Loon and Soler* [2004] have obtained an effective diffusion coefficient for HTO perpendicular to bedding of $D_e = \varepsilon\ D_p = 6.1 \times 10^{-12} \pm 0.6 \times 10^{-12}$ m^2 s^{-1} (22 ± 2°C). With a water-filled porosity ε of 0.12 ± 0.02 m^3 m^{-3}, a pore diffusion coefficient D_p of about $5.0 \times 10^{-11} \pm 1.0 \times 10^{-11}$ m^2 s^{-1} at 22 ± 2°C can be deduced. At Benken, the in situ temperature in the Opalinus Clay is and has been for the last several millions of years about 35 to 40°C [*Nagra*, 2001], with somewhat lower

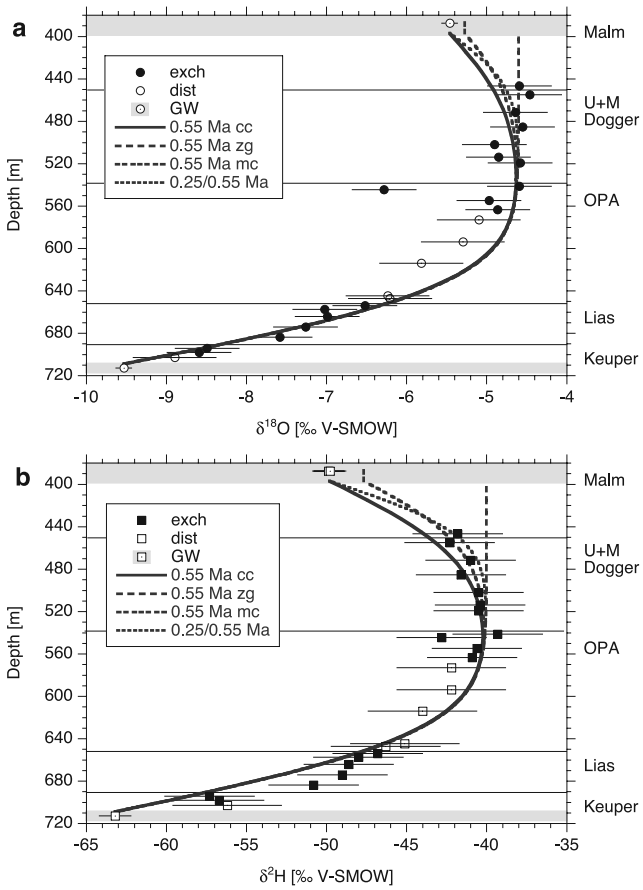

Figure 8. Effect of variation of the Malm boundary condition on the calculated profiles for (a) $\delta^{18}O$ and (b) $\delta^{2}H$. Here cc, constant concentration (base case); zg, zero gradient; mc, mixing cell; 0.25/0.55 Ma, cc but lower evolution time (or lower diffusion coefficient) in upper part of profile.

temperatures in the upper part of the low-permeability zones. The laboratory diffusion coefficient D_p at this temperature is about $1.0 \times 10^{-10} \pm 0.2 \times 10^{-10}$ m^2 s^{-1} [*Van Loon and Soler*, 2004], i.e., twice that at room temperature. With that value, an evolution time of about 0.55 ± 0.1 Ma was estimated for $\xi = 42$ m, where the error covers only the uncertainty of the laboratory diffusion coefficient D_p. For somewhat lower temperatures as in the upper part of the low-permeability zones, a slightly larger time would be estimated. An evolution time on the order of 0.5 Ma seems plausible when compared with the maximum time frame of about 1.8 Ma that was set by geologic and geochemical evidence. Conversely, the agreement between estimated evolution time and geologic evidence indicates that to an order of magnitude, laboratory diffusion coefficients can be considered as relevant on these much larger temporal and spatial scales.

[57] In the following, we will commonly indicate evolution times instead of values for ξ. All evolution times were calculated from ξ estimates with the above mentioned diffusion coefficient $D_p = 1.0 \times 10^{-10}$ m^2 s^{-1}. Of course, a different D_p value would, for the same ξ, lead to different evolution times, according to the relation $t = \xi^2/D_p$. A different D_p value requires, in addition, a scaling of the flushing rate (for calculations involving a mixing cell) according to the relation $\rho_1/D_{p1} = \rho_2/D_{p2}$, and a scaling of the velocity (in case of advective flow) according to $v_1/D_{p1} = v_2/D_{p2}$. Thus, if a lower diffusion coefficient of $D_p = 5.0 \times 10^{-11}$ m^2 s^{-1} is used, evolution times have to be doubled to get the same calculated values, if at the same time the flushing rate and the advective velocity are reduced by a factor of two.

[58] A closer look at Figure 7 reveals that a single calculation may not fit both data sets equally well. Indeed, from individual data sets we estimated a diffusion distance $\xi = 47$ m for $\delta^{18}O$ and $\xi = 36$ m for $\delta^{2}H$ (Figure 7, thin lines). The differences in the calculated curves are relatively small compared to the scatter of the data, but they would translate to a ratio of about 1.75 for the evolution times t (smaller time for ^2H) or for the pore diffusion coefficients D_p (smaller diffusion coefficient for ^2H), respectively. Different evolution times t due to nonsimultaneous change of boundary conditions for ^{18}O and ^2H are not plausible. Different diffusion coefficients D_p of ^2H and ^{18}O are, in principle, possible and could have various origins. A retarded diffusion of ^2H as compared to ^{18}O may result from slightly stronger enrichment of ^2H in interlayer or other strongly bound water, but such differences are expected to affect the ratio of diffusion coefficients only at the second or third decimal. Relative mass differences for ^{18}O in water as compared to ^2H in water may also lead to different diffusion coefficients. According to Graham's law applied for average species, this ratio is about 0.975, which means that ^{18}O would be retarded as compared to ^2H. Thus the relative mass differences cannot explain the findings. Interaction of ^{18}O of the pore water with oxygen of solids could be regarded as another possibility. Such interaction would include dissolution/precipitation reactions, as for instance calcite dissolution, and isotopic exchange between pore water and minerals. The pore water is in chemical equilibrium with and buffered by the surrounding rock [*Gimmi and Waber*, 2004]. Only minimal mass transfer induced by dissolution/precipitation reactions is required to preserve equilibrium along the chemical gradients toward the aquifers. Such small mass transfer could not account for observable changes in the pore water ^{18}O or ^2H concentrations. Isotopic exchange can also be excluded because such reactions are extremely slow (on the order of tens of millions of years) at the in situ temperatures present in the formation since the last burial. More important, both processes, reactions and isotopic exchange, would slow down the diffusion of ^{18}O as compared to ^2H, in contrast to what is observed.

[59] On the basis of these considerations, we believe that the different ξ values for ^{18}O and ^2H mainly reflect uncertainties of the data and of the modeling approach. The factor 1.75 may just give an estimate of uncertainty for calculated evolution times.

5.2. Variation of Malm Boundary Condition

[60] The upper boundary influences calculated values in the upper part of the profiles but has no effect on the estimated ξ or t. This is illustrated in Figure 8. Calculations for a zero-gradient upper boundary condition seem to describe the ^{18}O (but not the ^2H data) even better than the base case, but the same ξ as for a constant concentration at the Malm boundary was estimated. Using a mixing cell

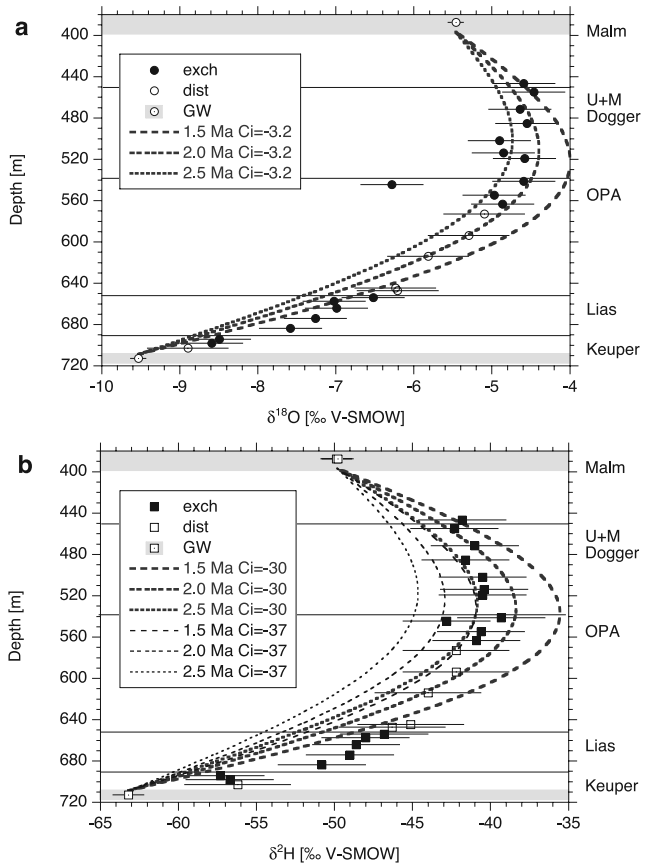

Figure 9. Influence of larger initial concentrations C_i (as compared to the base case) on simulated concentration profiles of (a) δ^{18}O and (b) δ^2H. The initial conditions used are shown in Figure 4.

boundary condition at the Malm interface led, depending on parameters, to profiles intermediate between those for a constant concentration and a zero gradient, but, again, always to the same value of ξ. Figure 8 also shows calculations for a constant concentration at the Malm boundary, but assuming a shorter evolution time or, correspondingly, a lower diffusion coefficient D_p for the upper part of the profile. The latter could originate from a somewhat lower porosity or lower temperature in the upper part of the profile.

[61] Since there are no data in the uppermost part of the Dogger units, it cannot be decided, which boundary condition is most appropriate for the Malm interface. However, for all tested conditions at the Malm interface, the major part of the profile, and thus the value of the estimated ξ or t, was determined by the lower boundary.

5.3. Variation of Initial Condition

[62] The effects of choosing larger initial concentrations are shown in Figure 9. The initial concentration for δ^{18}O was arbitrarily increased (toward the value of seawater) from −4.6‰ to −3.2‰. Approximate fits were obtained in this case for t ∼1.5 to 2.5 Ma ($\xi \sim 70$ to 90 m). The corresponding initial concentration for δ^2H was chosen in two ways. Firstly, it was chosen so that a similar agreement between data and calculations was obtained for the same values of t (initial value of −30‰, Figure 9b). As is obvious, the agreement between measurements and simulations is not satisfactory for any t. The calculated curves have generally a different shape. For shorter times, the deviations are especially large in the central regions, whereas for longer times, the data in the lower part are clearly underestimated. In addition, the ratio between the initial values of δ^2H and δ^{18}O (see Figure 4) is far from any local trend of the data and thus not very likely.

[63] Choosing an initial value for δ^2H according to the local trend of pore water composition, that is the ratio of the δ^2H and δ^{18}O values in the upper part of the profile, which might be more reasonable, gives an even worse picture (Figure 9b, initial value of −37‰). For an evolution time t of 1.5–2.5 Ma, as obtained for ^{18}O, the calculated curves all underestimate the measured data significantly. No value of ξ or t could be found in this case that led to a satisfying match with the data.

[64] These observations led to the conclusion that today's maximum values in the upper part of the profile represent approximately initial values prior to the activation of the Keuper aquifer. Even if we did not explicitly test nonuniform initial concentrations, the relatively good comparisons shown in Figure 7 are consistent with our assumption that initial values, before the relatively late drop in isotope values in the Keuper aquifer, were more or less constant throughout the formations.

5.4. Variation of Keuper Boundary Condition

[65] Assuming a constant concentration at the Keuper boundary as in the base case implies that the δ values dropped instantaneously. A more gradual decrease can be obtained with the mixing cell boundary condition, depending on the values of the flushing rate ρ and the equivalent height ζ. In the following simulations, ζ was set equal to 10 m, which roughly represents equivalent aquifer thickness.

[66] Figure 10a shows calculated δ^{18}O profiles for a flushing rate ρ of 2×10^{-5} yr^{-1}. For this case, the time in which the aquifer element is flushed once with external water equals 5×10^4 years. This time is relatively short compared to diffusion times of the order of 5×10^5 years as estimated from the base case. Consequently, the simulated concentration drop in the Keuper occurs relatively rapidly. An approximate fit was obtained for an evolution time of about 1 Ma (ξ = 56 m) with this boundary condition. If the δ values of the inflowing water are like those observed today, that is −9.53‰, the concentration in the Keuper is overestimated even at larger evolution times (Figure 10a, thick lines). If the inflow values are decreased to −10 or −10.5‰ for ^{18}O (Figure 10a, thin lines), the comparison becomes generally rather good, even slightly better than for the base case. Such an isotope composition would still be consistent with the climatic conditions during infiltration as derived from the measured values of the Keuper groundwater.

[67] Increasing the flushing rate to large values leads finally to an instantaneous concentration drop like in the base case. Reducing the flushing rate, on the other hand, generally produced worse agreement between measurements and calculations, as is illustrated for δ^{18}O and $\rho = 2 \times 10^{-6}$ yr^{-1} in Figure 10b. If inflow concentrations like those observed today are used, concentrations drop too slowly at the lower boundary, and propagate too far up into the overlying Dogger units. Deriving a (rather poor) match of the data at low flushing rates of 2×10^{-6} yr^{-1} or

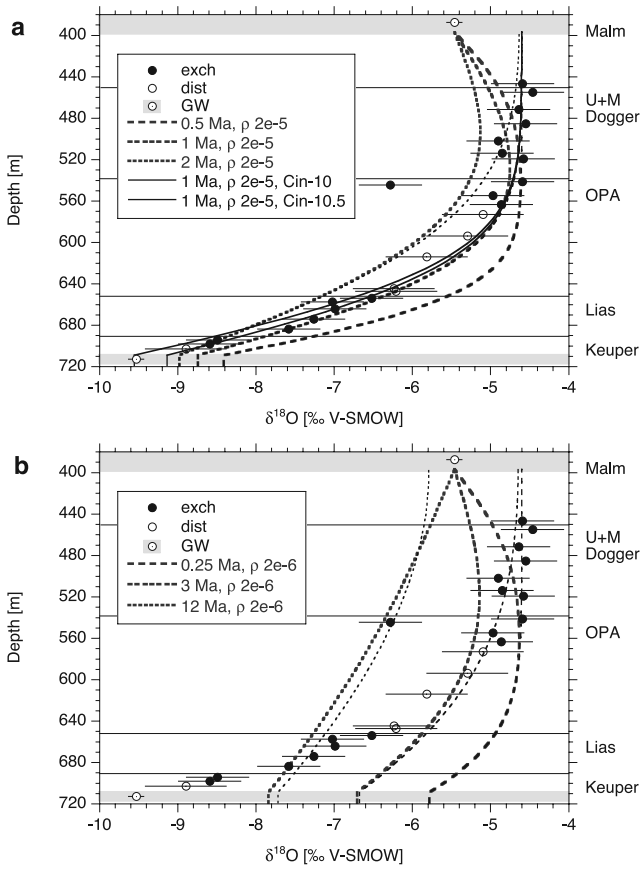

Figure 10. Simulated concentration profiles of $\delta^{18}O$ for a mixing cell boundary condition at the Keuper aquifer. (a) Flushing rate ρ of 2×10^{-5} yr^{-1}. Thick lines, Keuper inflow concentration C_{in} of -9.53‰ and constant concentration at upper boundary (at three evolution times); thin solid lines, Keuper inflow concentration of -10.0 and -10.5‰ at an evolution time of 1 Myr; thin dashed lines, as for thick lines but for zero gradient at upper boundary. (b) Flushing rate ρ of 2×10^{-6} yr^{-1}, Keuper inflow concentration C_{in} of -9.53‰ (at three evolution times). Thick lines, constant concentration at the upper boundary; thin lines, zero gradient at the upper boundary.

2×10^{-7} yr^{-1} requires unreasonably low isotope compositions of the inflowing water of -20 or -120 ‰, respectively, for $\delta^{18}O$ (not shown). Thus such low flushing rates were rejected.

[68] Mixing cell boundary conditions can of course only represent a limited range of temporal development, and the corresponding parameters, notably the flushing rate, should be interpreted with care. However, the simulations with a mixing cell boundary at the Keuper interface indicate clearly that the isotope contents in this aquifer dropped relatively rapidly. In the base case, where an instantaneous drop was assumed, the evolution time was estimated to be about 0.5 Ma. For cases with more gradual concentration decreases, the estimated evolution times increase to about 1 Ma at most.

5.5. Combined Effects of Boundary and Initial Conditions

[69] In most cases so far only one boundary or initial condition at a time was varied from the base case. To test combined effects, we compared $\delta^{18}O$ data with simulations for zero gradient at the upper boundary, increased initial values of -3.2‰ or -3‰ (closer to seawater), and constant or time-dependent values at the lower boundary. The results (Figures 10 and 11) corroborate the conclusions drawn above based on individual variations of boundary or initial conditions. In Figure 10, calculations for a mixing cell condition at the Keuper aquifer and a zero-gradient condition at the Malm interface are shown in addition to those with constant concentration at the Malm interface. Again it became obvious that the upper boundary condition has only a minor impact, especially if the lower part of the profile is described adequately. Figure 11 demonstrates that, for an increased initial concentration of -3.2‰ or -3‰, respectively, no reasonable fit can be obtained for any diffusion distance ξ, irrespective of the combination of upper and lower boundary conditions.

5.6. Influence of Advection

[70] Upward or downward advective flow across the Dogger units may have occurred during certain times, and at certain locations. To obtain an idea about the possible influence of advection, we investigated the simplified case of constant upward or downward flow. For preset values of the velocity v (or v/D_p, respectively), we estimated ξ (or the evolution time t, respectively) by minimizing the mean

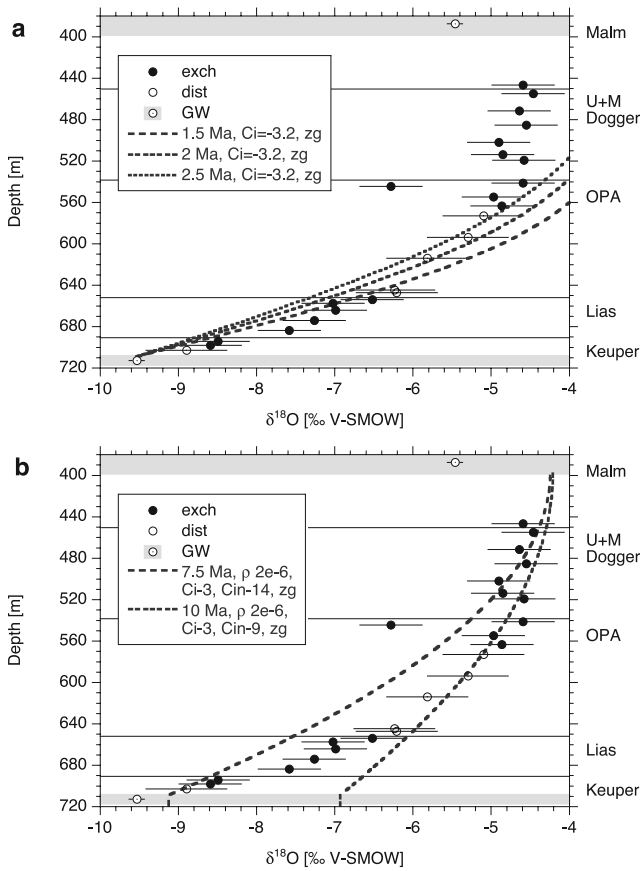

Figure 11. Calculations for $\delta^{18}O$ for combined effects of increased initial concentration ($C_i = -3.2$‰ or -3‰), zero gradient (zg) upper boundary condition, and (a) constant concentration or (b) mixing cell (with ρ and C_{in} as indicated) lower boundary condition.

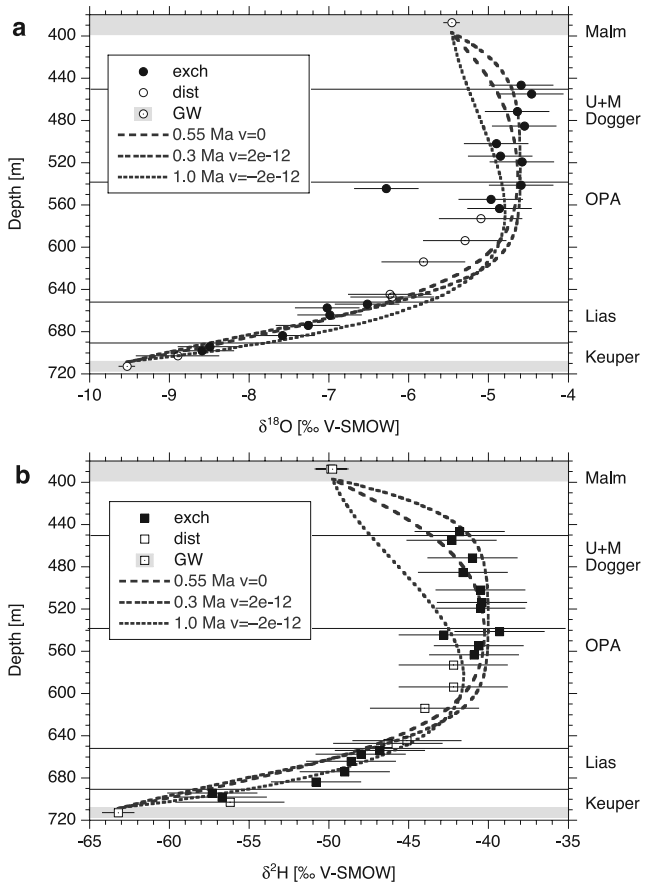

Figure 12. Influence of relatively small upward or downward advective velocity, as compared to pure diffusion, on fitted concentration profiles of (a) $\delta^{18}O$ and (b) $\delta^{2}H$. Here $v > 0$ indicates upward velocity, $v < 0$ indicates downward velocity, and $v = 0$ indicates pure diffusion.

squared deviations $\Delta = \chi^2/n$ between calculations and measurements for the combined data sets.

[71] Figure 12 shows the best fit curves for relatively small, constant velocities $v = 2 \times 10^{-12}$ m s^{-1} (upward) and $v = -2 \times 10^{-12}$ m s^{-1} (downward), together with the best fit curve of the base case ($v = 0$ m s^{-1}). It can be seen that for such low velocities, the deviations from the base case are relatively small, especially for upward flow. However, in both cases the mean squared deviation per data point, Δ, is somewhat larger than for the base case with $v = 0$ m s^{-1} (see following paragraph). For velocities $|v| = 2 \times 10^{-11}$ m s^{-1}, the differences to the base case are already very large (not shown), and no reasonable fits could be obtained at all, which is also reflected in the large Δ values.

[72] A summary over minimum average deviations Δ between measurements and simulations for various advective velocities $|v|$ is presented in Figure 13. The numbers in the plot denote the evolution times estimated from ξ with the laboratory diffusion coefficient at 40°C of 1×10^{-10} m^2 s^{-1}. Using this value for all velocities means that we neglected hydrodynamic dispersion, which will not contribute much at these low velocities anyway. In general, upward velocity led to smaller, and downward velocity to larger, evolution times. For velocities smaller than about $v = 2 \times 10^{-12}$ m s^{-1} the estimated evolution times varied only over a small range (about 0.3–1.0 Ma). For larger velocities, clearly smaller or larger evolution times were estimated, but the fits were so poor that these values should not be considered.

[73] The relative importance of advective versus diffusive or dispersive mass transfer can be estimated from the Peclet number $Pe = |v|L/D_p$. If this dimensionless number is smaller than about unity, advection is negligible and diffusion dominates over the length scale L. The corresponding limit for $|v|$ equals in our system with $L \sim 300$ m and $D_p \sim 1 \times 10^{-10}$ m^2 s^{-1} about 3.3×10^{-13} m s^{-1}, and is indicated by the vertical line in Figure 13. Overall, the smallest minimum deviations Δ were found to the left of this line, where diffusion dominates. When advective flow also contributed to transport, the mean squared deviations Δ increased, especially for downward flow.

[74] It is interesting to compare velocities used in the simulations with those estimated from the present-day hydraulic situation in this region [*Nagra*, 2002]. The hydraulic gradient between the Keuper and Malm aquifer of about -0.5 m m^{-1} points today to upward flow, if we neglect the slight overpressures within the low-permeability zones. With a hydraulic conductivity perpendicular to the layering of about 2×10^{-14} m s^{-1} and a generic water-filled porosity of about 0.1 m^3 m^{-3}, one calculates an advective velocity of 1×10^{-13} m s^{-1}. This value leads to $Pe = 0.3$, which also indicates that today advection is hardly an important transport mechanism.

[75] Assuming spatially and temporally constant flow over the last million years is a very simplified scenario. Loading and unloading of the surface with ice following glaciation may have caused variable horizontal or vertical water flow. However, since the Dogger units were once covered with about 1000 m of sediments more than today [*Nagra*, 2002, p. 56ff] and thus are considered to be overconsolidated, it is unlikely that glaciation has caused large changes of porosity and advective flow. Horizontal strain may also lead to upward and downward flow of water.

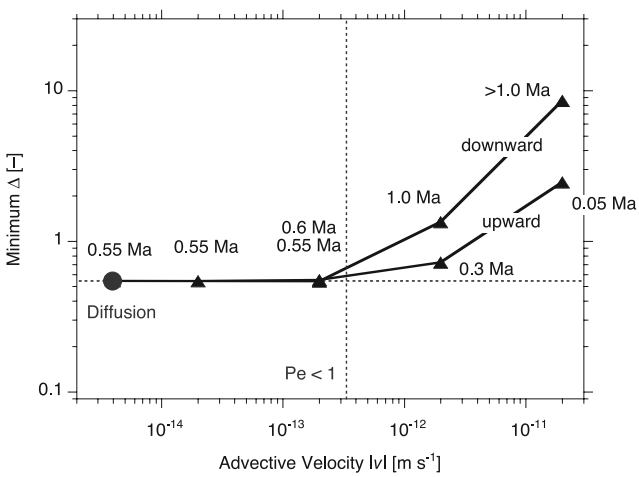

Figure 13. Calculated minimum average deviations Δ between measurements and simulation (see equation (13)) versus absolute values of advective velocity v for boundary and initial conditions of the base case. Labels next to points or triangles indicate evolution times for upward or downward flow. The point on the left and the horizontal line indicate minimum Δ for pure diffusion.

Calculations of velocities based on present-day fluid pressures within the Dogger units led to values $|v|$ between zero and about 9×10^{-13} m s^{-1} (G. Kosakowski, personal communication, 2001), with maximum values occurring only right at the Malm and Keuper interfaces. Again, such velocities have only a very small effect on simulated isotope profiles, as was verified with a numerical calculation.

[76] Figure 13 clearly shows that the assumption of diffusion dominated isotope exchange leads to minimal deviations between measured data and simulations. Diffusion dominated means, that advection is either absent or so small, that it hardly influences the calculations. The latter is true in the investigated system for velocities smaller than about 3×10^{-13} m s^{-1}. Conversely, we conclude from Figure 13 that advection did not leave any detectable signature in the isotope profiles observed today at Benken. This conclusion is also supported by the low velocities estimated from measured hydraulic conductivities and present-day hydraulic gradients across, or overpressures within, the Dogger and Lias units.

6. Summary and Conclusions

[77] We determined values of δ^{18}O and δ^{2}H in the pore fluid of low-permeability formations at Benken in northeastern Switzerland. The formations are of Jurassic and uppermost Triassic age, and they were sampled at depths between about 400 and 700 m. A new technique based on diffusive vapor exchange of isotopes [*Rübel et al.*, 2002] was used to obtain the pore water isotopic composition from the rock samples. It led to values consistent with those from squeezing, whereas the conventional vacuum distillation method was inaccurate for the argillaceous rocks. It suffered from incomplete distillation, which results in fractionation effects such that measured values were depleted in the heavy isotopes with respect to those in situ. Similar observations were made by *Kelln et al.* [2001], *Rübel et al.* [2002], *Pearson et al.* [2003], and *Savoye et al.* [2006], whereas *Patriarche et al.* [2004a] used data from vacuum distillation at 50°C without a comparison with other data.

[78] The observed profiles provide a unique opportunity to evaluate transport through the Jurassic sedimentary rocks on large spatial and temporal scales. They seem to be influenced mainly by mass exchange with the underlying Keuper aquifer. To quantify these processes, we performed a series of advective-diffusive transport simulations. In accordance with the hydrogeological history, we varied the initial and boundary conditions, as well as model parameters.

[79] The conclusions from the simulations of the stable water isotopes data are the following.

[80] 1. Initial isotope ratios before the onset of flow in the local Keuper aquifer were shifted to lower values with respect to the initial marine pore water. They correspond to values measured in the upper and middle part of the Dogger units.

[81] 2. Some time after activation of flow, values in the Keuper aquifer appear to have decreased rapidly to meteoric values. A slow concentration decrease cannot reproduce the observed data well.

[82] 3. Conditions at the Malm boundary had only a small effect on the observed profiles. The available data do not allow discrimination between different possible upper boundary conditions.

[83] 4. The profiles appear to have evolved mainly via molecular diffusion. No signature of advective flow could be detected.

[84] 5. Depending on boundary conditions, a diffusion distance $\xi = (tD_p)^{0.5}$ of about 42 to 56 m was estimated. This corresponds to evolution times of about 0.5–1 Ma based on a laboratory diffusion coefficient D_p at 40°C [*Van Loon and Soler*, 2004] of 1×10^{-10} m^2 s^{-1}.

[85] 6. Additional uncertainty about relevant temperatures and processes (e.g., slight variability of porosities and diffusion coefficients) may increase the estimated span of evolution to about 0.2–1.5 Ma.

[86] These evolution times, estimated using laboratory diffusion coefficients, are plausible when compared to geological and geochemical evidence (activation of Keuper flow systems in this area at about 2 Ma B.P., residence times of Keuper water much longer than 25 ka but less than 2.6 Ma). Also, no advective signatures could be detected in the isotope profiles, in accord with the low hydraulic conductivities determined in the laboratory and via borehole tests, and with the present-day hydraulic gradients. These findings allow us to draw an additional, more general conclusion: Parameters of the investigated Jurassic sedimentary rocks, such as diffusion coefficients and hydraulic conductivities, that were measured on small spatial and temporal scales (centimeters or meters, months), seem to be applicable at larger scales (tens of meters, millions of years), at least to within an order of magnitude.

[87] Isotope profiles dominated by diffusion were also found in surficial Quaternary aquitards [*Desaulniers et al.*, 1981; *Remenda et al.*, 1996; *Hendry and Wassenaar*, 1999], or at the interface toward an underlying Cretaceous clay [*Hendry and Wassenaar*, 1999]. In those cases, the formations were smaller and the profiles developed over considerably shorter times of about 10 to 30 ka, compared to our evolution time of about 0.5 to 1 Ma. The long time span of dominating diffusion points out the low hydraulic conductivity of the investigated Jurassic formations. Isotope signatures that indicate long times of diffusion-dominated transport were also found by *Rübel et al.* [2002] and *Patriarche et al.* [2004a]. The former considered 10 Ma, but started from seawater conditions without accounting for the regional and local paleohydrology in detail. The latter, in trying to model the evolution of the profiles over 53 Ma, had to make assumptions about the climatic and paleohydrologic conditions that are only poorly supported, and neglected advection at all except for the last 3 Ma.

[88] *Desaulniers et al.* [1981] and *Remenda et al.* [1996] concluded that conventional testing tends to overestimate hydraulic conductivities of aquitards. We can neither support nor reject this statement, because we did not observe any advective signature in the isotope profiles. However, we conclude that the hydraulic conductivities obtained from borehole tests at Benken can be considered as an upper limit for the formation; for clearly larger values, advective signatures would be expected in the isotope profiles, based on present-day hydraulic gradients. *Patriarche et al.* [2004a] compared diffusion coefficients estimated from δ^{2}H profiles with values obtained on small samples. In contrast to our study, their estimated (heterogeneous) coefficients turned

out to be very sensitive with regard to the applied boundary conditions; they were either similar or more than one order of magnitude larger than the small-scale values. Thus they could not draw a clear conclusion about the use of small-scale diffusion coefficients at large scales. At our site, the geology is considerably simpler, and the isotope profiles seem to be dominated by a relatively late event. These conditions clearly facilitated the interpretation of the stable isotope profiles at Benken.

[89] **Acknowledgments.** These investigations were funded by Nagra, the National Cooperative for the Disposal of Radioactive Waste, Switzerland. We have greatly benefited from intensive scientific discussions with Martin Mazurek (University of Bern) and other colleagues from Bern and from the Paul Scherrer Institut. We also wish to express our thanks to Ghislain de Marsily (University Paris VI) for very constructive discussions about the topics, as well as to F. Joe Pearson (Groundwater Geochemistry) for important editorial and scientific comments. We acknowledge the comments of three reviewers, which were very helpful in improving the manuscript.

References

Balderer, W. (1990), Hydrogeologische Charakterisierung der Grundwasservorkommen innerhalb der Molasse in der Nordostschweiz aufgrund von hydrochemischen und Isotopenuntersuchungen, *Steirische Beitr. Hydrogeol.*, *41*, 35–104.

Bertleff, B., and R. Watzel (2002), Tiefe Aquifersysteme im südwestdeutschen Molassebecken: Eine umfassende hydrogeologische Analyse als Grundlage eines zukünftigen Quantitäts- und Qualitätsmanagements, *Abh. Landesamt Geol. Rohstoffe Bergbau Baden Wuerttemberg*, *15*, 75–90.

Birkhäuser, P., P. Roth, B. Meier, and H. Naef (2001), 3D-Seismik: Räumliche Erkundung der mesozoischen Sedimentschichten im Zürcher Weinland, *Nagra Tech. Rep. NTB 00-03*, Natl. Genossenschaft für die Lagerung radioaktiver Abfälle, Wettingen, Switzerland.

Desaulniers, D., J. Cherry, and P. Fritz (1981), Origin, age and movement of pore water in argillaceous quaternary deposits at four sites in southwestern Ontario, *J. Hydrol.*, *50*(1–3), 231–257.

Flury, M., and T. Gimmi (2002), Solute diffusion, in *Methods of Soil Analysis*, part 4, *Physical Methods*, edited by J. H. Dane, and G. C. Topp, pp. 1323–1351, Soil Sci. Soc. of Am., Madison, Wis.

Gimmi, T., and H. Flühler (1998), Mixing-cell boundary conditions and apparent mass balance errors for advective-dispersive solute transport, *J. Contam. Hydrol.*, *33*, 101–131.

Gimmi, T., and H. N. Waber (2004), Modelling of tracer profiles in pore water of argillaceous rocks in the Benken borehole: Stable water isotopes, chloride, and chlorine isotopes, *Nagra Tech. Rep. NTB 04-05*, Natl. Genossenschaft für die Lagerung radioaktiver Abfälle, Wettingen, Switzerland.

Gregory, R. T. (1991), Oxygen isotope history of seawater revisited: Timescales for boundary event changes in the oxygen isotope composition of seawater, in *Stable Isotope Geochemistry: A Tribute to Samuel Epstein*, edited by H. P. Taylor, J. R. O'Neil, and I. R. Kaplan, *Spec. Publ. Geochem. Soc.*, *3*, 65–76.

Hendry, M. J., and L. I. Wassenaar (1999), Implications of the distribution of δD in pore waters for groundwater flow and the timing of geologic events in a thick aquitard system, *Water Resour. Res.*, *35*, 1751–1760.

Hendry, M. J., C. J. Kelln, L. I. Wassenaar, and J. Shaw (2004), Characterizing the hydrogeology of a complex clay-rich aquitard system using detailed vertical profiles of the stable isotopes of water, *J. Hydrol.*, *293*, 47–56.

Jury, W. A., and K. Roth (1990), *Transfer Functions and Solute Movement Through Soil: Theory and Applications*, Springer, New York.

Kelln, C. J., L. I. Wassenaar, and M. J. Hendry (2001), Stable isotopes (δ^{18}O, δ^{2}H) of pore waters in clay-rich aquitards: A comparison and evaluation of measurement techniques, *Ground Water Monit. Rem.*, *21*(2), 108–116.

Mazurek, M., A. J. Hurford, and W. Leu (2006), Unravelling the multistage burial history of the Swiss Molasse Basin: Integration of apatite fission track, vitrinite reflectance and biomarker isomerisation analysis, *Basin Res.*, *18*, 27–50, doi:10.1111/j.1365-2117.2006.00286.x.

Nationale Genossenschaft für die Lagerung radioaktiver Abfälle (Nagra) (2001), Sondierbohrung Benken, Untersuchungsbericht, *Nagra Tech. Rep. NTB 00-01*, Wettingen, Switzerland.

Nationale Genossenschaft für die Lagerung radioaktiver Abfälle (Nagra) (2002), Projekt Opalinuston: Synthese der geowissenschaftlichen Untersuchungsergebnisse, *Nagra Tech. Rep. NTB 02-03*, Wettingen, Switzerland.

Patriarche, D., E. Ledoux, J.-L. Michelot, R. Simon-Coinçon, and S. Savoye (2004a), Diffusion as the main process for mass transport in very low water content argillites: 2. Fluid flow and mass transport modeling, *Water Resour. Res.*, *40*, W01517, doi:10.1029/2003WR002700.

Patriarche, D., J.-L. Michelot, E. Ledoux, and S. Savoye (2004b), Diffusion as the main process for mass transport in very low water content argillites: 1. Chloride as a natural tracer for mass transport—Diffusion coefficient and concentration measurements in interstitial water, *Water Resour. Res.*, *40*, W01516, doi:10.1029/2003WR002600.

Pearson, F. J., W. Balderer, H. H. Loosli, B. E. Lehmann, A. Matter, T. Peters, H. Schmassmann, and A. Gautschi (1991), *Applied Isotope Hydrogeology—A Case Study in Northern Switzerland, Stud. Environ. Sci.*, vol. 43, Elsevier, New York.

Pearson, F. J., D. Arcos, A. Bath, J.-Y. Boisson, A. M. Fernández, H. E. Gaebler, E. Gaucher, A. Gautschi, L. Griffault, P. Hernan, and H. N. Waber (2003), Mont Terri Project—Geochemistry of water in the Opalinus Clay formation at the Mont Terri Rock Laboratory, *Geol. Ser. 5*, Fed. Off. for Water and Geol., Bern.

Remenda, V. H., J. A. Cherry, and T. W. D. Edwards (1994), Isotopic composition of old ground water from Lake Agassiz: Implications for late Pleistocene climate, *Science*, *266*, 1975–1978.

Remenda, V. H., G. van der Kamp, and J. A. Cherry (1996), Use of vertical profiles of δ^{18}O to constrain estimates of hydraulic conductivity in a thick, unfractured aquitard, *Water Resour. Res.*, *32*(10), 2979–2987.

Rübel, A., C. Sonntag, J. Lippmann, A. Gautschi, and F. J. Pearson (2002), Solute transport in formations of very low permeability: Profiles of stable isotope and dissolved gas contents of the pore water in the Opalinus Clay, Mont Terri, Switzerland, *Geochim. Cosmochim. Acta*, *66*, 1311–1321.

Sacchi, E., J.-L. Michelot, H. Pitsch, P. Lalieux, and J-.F. Aranyossy (2001), Extraction of water and solutes from argillaceous rocks for geochemical characterisation: Methods, processes and current understanding, *Hydrogeol. J.*, *9*(1), 17–33.

Savoye, S., J.-L. Michelot, C. Wittebroodt, and M. V. Altinier (2006), Contribution of the diffusive exchange method to the characterization of pore-water in consolidated argillaceous rocks, *J. Contam. Hydrol.*, *86*, 87–104.

Trümpy, R. (1980), *Geology of Switzerland, part A, An Outline of the Geology of Switzerland*, Wepf, Basel, Switzerland.

Van Loon, L. R., and J. M. Soler (2004), Diffusion of HTO, $^{36}Cl^{-}$, $^{125}I^{-}$ and $^{22}Na^{+}$ in Opalinus Clay: Effect of confining pressure, sample orientation, sample depth and temperature, *PSI Rep. 04-03*, Paul Scherrer Inst., Villigen, Switzerland.

Villinger, E. (2003), Zur Paläogeographie von Alpenrhein und oberer Donau, *Z. Dtsch. Geol. Ges.*, *154*, 193–253.

A. Gautschi, National Cooperative for the Disposal of Radioactive Waste, Hardstrasse 73, CH-5430 Wettingen, Switzerland. (andreas.gautschi@nagra.ch)

T. Gimmi and H. N. Waber, Rock-Water Interaction, Institute of Geological Sciences, University of Bern, Baltzerstrasse 1–3, CH-3012 Bern, Switzerland. (thomas.gimmi@geo.unibe.ch; waber@geo.unibe.ch)

A. Rübel, GRS mbh, Theodor Heuss-Strasse 4, D-38122 Braunschweig, Germany. (rue@grs.de)